

RESEARCH

Open Access



# Dynamic deployment of H2A.Z positive nucleosome mediated transcriptomic plasticity within vascular smooth muscle cell

Chao Yu<sup>1,2</sup>, Jiaxin Huang<sup>3</sup>, Yan Wang<sup>1,4</sup>, Jia Song<sup>2\*</sup> and Wei Shen<sup>1,4\*</sup>

## Abstract

**Background** To maintain homeostasis in the mature human body, certain differentiated cells adopted high plasticity to refine their cellular functions. However, mechanisms that supported cellular plasticity still remained elusive. Here, through comprehensive transcriptomic and epigenetic studies of highly plastic vascular smooth muscle cells (SMCs), we aimed to decipher the chromatin basis that could mediate cellular plasticity.

**Results** In vascular smooth muscle cells, actively transcribed and highly adjustable genes tended to be associated with a continuously accessible region downstream of transcription start site (CAR-downTSS). This CAR-downTSS was located beyond the classic RNA polymerase II paused region, accessible at mono-nucleosome level and incorporated with histone variant H2A.Z. Depletion of H2A.Z reduced active histone modifications within CAR-downTSS, impaired RNA polymerase II transpassing when cells were stimulated, and consequently inhibited the ability of CAR-downTSS-associated genes to adjust their expression. Further in vitro and in vivo studies verified that this CAR-downTSS could be dynamically re-deployed onto different genes in vascular SMCs, whereas it was deployed in smaller quantities and remained quantitatively stable on genome within the quiescent cardiomyocytes.

**Conclusions** Vascular SMCs dynamically deployed H2A.Z-positive nucleosomes extending continuously downstream transcription start sites on different genes to support their transcriptional adjustability, which served as an important mechanism mediating cellular plasticity.

**Keywords** Histone variant H2A.Z, Downstream of TSS, Transcriptional plasticity, Vascular SMC, Vascular homeostasis

## Background

Within the mature human body, certain differentiated cells exhibit high levels of plasticity to refine cellular functions and maintain homeostasis. One well-known example is the plastic vascular smooth muscle cells (SMCs). Unlike the quiescent cardiomyocytes that also reside within the circulatory system [1, 2], vascular SMCs can de-differentiate and resume cell proliferation to repair tissue damage [3]. While, this reparative process could be misdirected in the presence of hostile blood environment (such as hyperlipidemia or hypertension), which would lead to the transformation of vascular SMCs into various

\*Correspondence:

Jia Song

tjsongjia@tust.edu.cn

Wei Shen

shenwei@xmu.edu.cn; shenwei@xmheart.com

<sup>1</sup>Institute of Cardiovascular Disease, Xiamen Cardiovascular Hospital of Xiamen University, School of Medicine, Xiamen University, Xiamen, China

<sup>2</sup>College of Biotechnology, Tianjin University of Science & Technology, Tianjin, China

<sup>3</sup>Center for Diagnostics and Therapeutics, Amoytop Biotech Inc, Xiamen, China

<sup>4</sup>Fujian Branch of National Clinical Research Center for Cardiovascular Diseases, Xiamen, China



© The Author(s) 2025. **Open Access** This article is licensed under a Creative Commons Attribution-NonCommercial-NoDerivatives 4.0 International License, which permits any non-commercial use, sharing, distribution and reproduction in any medium or format, as long as you give appropriate credit to the original author(s) and the source, provide a link to the Creative Commons licence, and indicate if you modified the licensed material. You do not have permission under this licence to share adapted material derived from this article or parts of it. The images or other third party material in this article are included in the article's Creative Commons licence, unless indicated otherwise in a credit line to the material. If material is not included in the article's Creative Commons licence and your intended use is not permitted by statutory regulation or exceeds the permitted use, you will need to obtain permission directly from the copyright holder. To view a copy of this licence, visit <http://creativecommons.org/licenses/by-nc-nd/4.0/>.

destructive phenotypes (such as macrophage-like or osteogenic-like cells) [4–6]. These SMC-derived destructive cell types further drive the development of most vascular diseases [7–11]. Although the plastic nature and disease-causing role of vascular SMCs have been well documented, the cellular and molecular mechanisms that mediate their plasticity remain elusive.

The plastic behavior of vascular SMCs is accompanied by flexible re-adjustment of genes' transcription. Gene transcription is known to be regulated by transcription factors, co-factors and other regulatory elements that ultimately converge at gene's promoter [12]. As a genomic region spanning a gene's transcription start site (TSS), promoter accepts regulatory factors and RNA polymerase that catalyzes the transcription of DNA into RNA [13–15]. The level of this transcription activity is further influenced by the status of nucleosomes, the basic units in which DNA wraps around an histone octamer composed of H2A, H2B, H3 and H4 proteins [16]. Various histone protein modifications can fine-tune transcription activities [17], and replacement of canonical histone proteins with their variants has significant impacts on transcription as well [18]. One most studied histone variant, H2A.Z, plays essential functions on establishing an RNA polymerase II paused region immediately downstream of TSS, which is critical for quick transcriptional initiation [19]. The presence of H2A.Z may extend further downstream of TSS, while its function in these regions remains unclear.

Here, through systematic transcriptomic and epigenetic studies, we found that H2A.Z was incorporated into a continuously accessible region downstream of TSS (CAR-downTSS), where it maintained active histone modifications, mediated RNA polymerase II transpassing within CAR-downTSS, and functionally supported transcriptional adjustability of CAR-downTSS-associated genes. Further comparative studies revealed CAR-downTSS could be dynamically deployed onto various genes in vascular SMCs, whereas it was deployed in smaller quantities and remained quantitatively stable on genome of quiescent cardiomyocytes. Therefore, dynamic adaptation of H2A.Z-incorporated CAR-downTSS likely served as an important mechanism mediating cellular plasticity.

## Methods

### Single-cell ATAC-seq (scATAC-seq) of human aortic media

The intima and adventitia layers of the isolated human aorta were surgically removed, leaving only the media layer for nucleus retrieval. The retrieved cell nucleus suspension was then used to construct the scATAC-Seq library using Chromium Next GEM Single Cell ATAC Reagent Kit v2 (10x Genomics, 1000390), and 20 gigabases of sequencing data were eventually generated. The raw data were first processed with *cellranger-atac* [20],

and further analyzed using the R packages *Seurat* [21] and *Signac* [22] to examine chromatin accessibility patterns at single-cell level.

### Bulk ATAC-Seq

The ATAC-Seq library was constructed using the Hyperactive ATAC-Seq Library Prep Kit for Illumina (Vazyme, TD711) following the manufacturer's instructions. For each experiment, 10 000 cells were collected for nucleus retrieval and library construction, and 6 to 9 gigabases of sequencing data were generated for each library. The raw data were processed using following packages for downstream analysis: *fastp* [23] for data cleaning, *Bowtie2* [24] for mapping, *SAMtools* [25] for file conversion and indexing, and *deepTools* [26] for k-means analysis.

### Cut&Tag sequencing

The Cut&Tag sequencing library was constructed using the Hyperactive Universal Cut&Tag Assay Kit for Illumina Pro (Vazyme, TD904) following the manufacturer's instructions. To locate the genomic positions of targeted proteins, we used the following primary antibodies: anti-H3K27ac antibody (Abcam, ab4729), anti-H3K4me3 antibody (Abcam, ab213224), anti-H3K27me3 antibody (Abcam, ab192985), anti-H3K9me3 antibody (Abcam, ab176916), anti-H2A.Z antibody (Abcam, ab4174), and anti-Pol II antibody (Abcam, ab238146). 6 gigabases of sequencing data were generated for each library and processed using the same packages as those used for ATAC-Seq data analysis.

### Bulk RNA-Seq

Total RNA was extracted using TRIzol reagent, and poly(A)-tailed RNA was further enriched for RNA-Seq library construction. 6 gigabases of sequencing data were generated for each library, which were processed using the following packages: *STAR* [27] for mapping, *HTSeq-count* [28] for gene counting, and *DESeq2* [29] for detecting differentially expressed genes. Differentially expressed genes were defined as those having an adjusted  $p$ -value  $< 0.05$  and absolute  $\log_2$  (fold change)  $> 1$ .

### Principal component analysis (PCA)

PCA was performed to assess the transcriptomic variance among vascular SMCs. The gene expression values were normalized, and genes with mean counts greater than 100 were included in the PCA. The analytic and plotting were performed using R language in RStudio.

### Calculation of promoter accessibility

The promoter was defined as 2000 bp upstream and downstream of a gene's transcription start site, and ATAC-Seq reads falling within this region were extracted for further analysis. During the correlation analysis

between promoter accessibility and gene expression or expression changes, ATAC-Seq reads within promoter regions were counted using *HTSeq-count*.

### Correlation analysis

Pearson correlation analysis was performed to calculate correlation coefficients. Comparisons were made between two sets of RNA-Seq data, one RNA-Seq and one ATAC-Seq, or two sets of ATAC-Seq data. When correlation between ATAC-Seq datasets was analyzed, a subset of cell population from scATAC-Seq was extracted to select cells pertaining CAR-downTSS on gene *KCNJ2*.

### Fragment size Estimation

ATAC-Seq or Cut&Tag sequencing reads falling within specific genomic regions were extracted, and the *bamPE-FragmentSize* algorithm from *deepTools* [26] was used to calculate the size of DNA fragments generated by Tn5-mediated fragmentation. The resulting data were further processed by R in RStudio to generate fragment size distribution plots.

### ShRNA knockdown

shRNA targeting specific genes was inserted into the pLKO.1 vector. Lentiviruses were subsequently produced by co-transfecting the vector with psPAX2 and pMD2.G. Successfully infected cells were selected by continuous culturing with puromycin. The knockdown efficiency of the shRNA was verified at both mRNA and protein level. The shRNA sequences used in this study were as follows: 5'-ACTTGAAGGTAAAGCGTATTACTCGAGTAATACGCTTTACCTTCAAGT-3' targeting rat *H2az1*, 5'-TAGGGCCCAAGAAAGAAATTACTCGAGTAATTTCTTTCTTGGGCCCTA-3' targeting rat *Srcap*, and 5'-GCTTCAAAGAAGCTATTGATTCTCGAGAATCAATAGCTTCTTTGAAGC-3' targeting human *H2AZ1*.

### qRT-PCR tests

RNA was extracted using TRIzol reagent according to the manufacturer's instructions and then reverse transcribed into cDNA for quantitative PCR. Each experiment was performed with duplicate or triplicate biological replicates, and the results are presented as the means  $\pm$  SDs. Student's *t*-tests were performed to assess the significance of differences, with results are presented as \* for  $p < 0.05$ , \*\* for  $p < 0.005$  and \*\*\* for  $p < 0.001$ .

### Immunostaining

Cultured cells were seeded into an 8-well chamber (ibidi, 80841) and maintained under standard culture conditions. Briefly, DMEM (Procell, PM150210) supplemented with 10% FBS (Gibco, 10099) and 1% penicillin-streptomycin (Thermo, 15140122) was used as the culture medium, and 5% CO<sub>2</sub> was maintained as the incubator

condition. Immunostaining was performed on these cells using an anti-H2a.z primary antibody (Abcam, ab4174) and an anti-rabbit secondary antibody conjugated with Alexa Fluor 594 (Invitrogen, A11012). The stained cells were further imaged using a confocal microscope (Leica, Stellaris 5) and images were assembled using Adobe Photoshop.

### Ethnic statement

The use of live animals for primary cell culture was approved by the Experimental Animal Care and Use Committee at Xiamen University and conformed to the Guide for the Care and Use of Laboratory Animals published by the U.S. National Institutes of Health. The use of human aorta sample was reviewed and approved by the Ethics Committee at Xiamen Cardiovascular Hospital of Xiamen University.

## Results

### Human vascular SMCs could adapt to highly variable transcriptomes with gene expression being drastically re-adjusted

To quantitatively assess the plasticity of vascular SMCs, we profiled the transcriptome of one human aortic SMC line (hereafter HASMC1) before and after cholesterol treatment (a well-known condition that induces SMC to macrophage-like cell transformation [30]). The transcriptome change detected during this SMC to macrophage-like cell transformation was further used as a reference to assess transcriptomic variability among different human aortic SMCs (extracted from different individuals). These included a second line of human aortic SMC (hereafter HASMC2) and another 5 human aortic SMCs whose RNA-Seq datasets were recently released into public database (hereafter referred as to pub h1 to h5). As expected, significant transcriptome changes were detected during SMC to macrophage-like cell transformation (Supplemental Fig. 1A-1B). While, this change was relatively minor compared to transcriptome variances detected among HASMC1-2 and pub h1-h5, as shown by the principal component analysis (PCA) result (Fig. 1A).

The high variability of SMCs' transcriptome was reflected not only by highly variable expression of SMC marker gene *ACTA2* (ranged from 458 to 21 656) and *TAGLN* (ranged from 194 to 45 598) (Fig. 1B), but also by genome-wide re-adjustments beyond classic marker genes as indicated by low correlation coefficients calculated from whole transcriptome profiles (Fig. 1C). To further clarify whether this transcriptome variability was attributed to human genome variances (such as the variable Major Histocompatibility Complex region on chromosome 6) [31, 32]) that were known to present among different individuals, we removed RNA-Seq

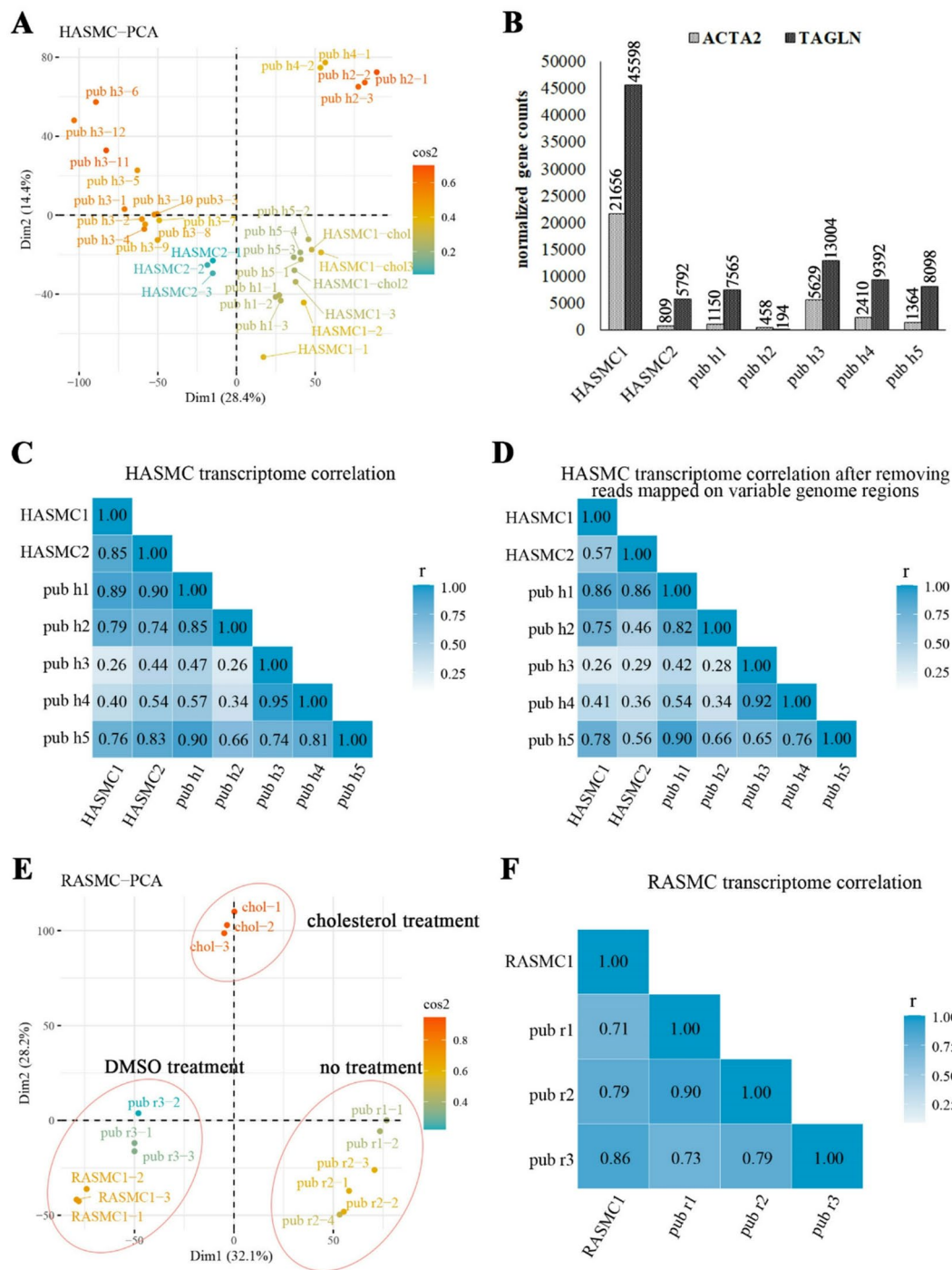


**Fig. 1** Human vascular SMCs could adapt to highly variable transcriptomes with gene expression being drastically re-adjusted. **(A)** PCA plot showing transcriptomic differences among HASMC1-2 and pub h1-h5. **(B)** Bar plot showing normalized gene counts for SMC marker gene *ACTA2* and *TAGLN* within HASMC1-2 and pub h1-h5. **(C)** Heatmap showing pairwise Pearson correlation coefficients among HASMC1-2 and pub h1-h5. **(D)** Heatmap showing pairwise Pearson correlation coefficients among HASMC1-2 and pub h1-h5 after removing sequencing reads mapped to variable regions of the human genome. **(E)** PCA plot showing the transcriptomic differences among RASMC1 and pub r1-r3. **(F)** Heatmap showing pairwise Pearson correlation coefficients among RASMC1 and pub r1-r3

reads mapped to all variable genome regions (total of 681 genomic regions collected in ensemble human genome assembly) (Supplemental Fig. 1C). The remaining RNA-Seq reads mapped to stable human genomes resulted in

similar or slightly lower correlation coefficients (Fig. 1D), confirming SMCs' transcriptome variability was primarily contributed by genes' inherent ability to re-adjust their expression levels. While, this high transcriptome

variability among human vascular SMCs also made it become difficult or even mis-leading to conduct integrative genome study via including public datasets. To overcome this issue and more reliably summarize any consistent genomic pattern that supported vascular SMCs' plastic transcriptome, we looked into the classic model system *Rattus norvegicus* that shared stable genome, standardized breeding condition and large aortas for accurate vascular SMCs extraction. After profiling transcriptome of one rat aortic SMC line (hereafter RASMC1) before and after cholesterol treatment and comparing it with transcriptome profiles from another 3 rat aortic SMC lines (hereafter referred to as pub r1 to r3) whose RNA-Seq datasets were recently released, we found transcriptome differences among different batches of rat SMCs were relatively minor compared to treatment-induced changes (Fig. 1E). Correlation analysis also confirmed overall fine correlations of gene expressions among these rat SMCs lines (Fig. 1F), therefore this model system would likely offer better opportunities to summarize any consistent genomic pattern supporting vascular SMCs' plasticity.

#### **Highly adjustable gene tended to be associated with a continuously accessible region downstream of transcription start site (defined as CAR-downTSS)**

To identify genomic features that could mediate the plastic behavior of vascular SMCs, we profiled chromatin accessibility in RASMC1 via ATAC-Seq and focused our analysis on promoter regions that ultimately accept all regulatory elements to control gene expression. The promoter accessibility level (calculated as the summed accessibility within  $\pm 2000$  bps from TSS) was found to be un-correlated with gene expression levels in RASMC1 ( $r=0.127$ ) or pub r1 ( $r=0.151$ ) (Fig. 2A). Furthermore, genes' ability to change their expression, which were detected after cholesterol treatment, PDGF treatment (driving SMC proliferation and migration [33], public dataset detailed in supplemental method) and Pi treatment (driving osteogenic-like transformation [34], public dataset detailed in supplemental method), also showed no correlation with promoter accessibility level ( $r = -0.173$ ,  $-0.215$  and  $-0.226$  for cholesterol, PDGF and Pi treatment, respectively) (Fig. 2B). These results suggested more complex pattern that beyond overall accessibility level may exist within promoter region, contributing to gene expression regulation and transcriptional adjustability.

We then further examined accessibility patterns within promoter regions by performing k-means clustering on accessible regions, which resulted in 9 distinct accessible patterns characterized by their accessible levels and relative positions to TSS (Fig. 2C and D). The position of accessible regions within promoter was found to

influence both transcriptional levels and transcription adjustability. Genes associated with cluster 4 (accessibility far upstream of TSS) showed lower expression levels compared to genes associated with other accessibility patterns (Fig. 2E & supplemental Fig. 2A), and genes associated with cluster 3 (accessibility immediately downstream of TSS, resembling RNA polymerase II paused region) and cluster 5 (continuously accessible region further downstream of TSS, defined as CAR-downTSS) exhibited distinctively higher accumulative gene changes in gene expression after cholesterol treatment (Fig. 2F). Although fewer genes were associated with cluster 5 than with cluster 3 (514 genes vs. 748 genes), cluster 5 genes showed larger accumulative changes (Fig. 2F) and included genes such as *Enpp3*, *Relb* and *Nampt* (Fig. 2G), that were known to promote vascular SMC transformation [35–37]. The distinctive high expression changes among cluster 5 (CAR-downTSS) genes were also observed during PDGF- or Pi-induced transformations (Fig. 2H and I), although the specific genes with significant expression changes varied among the 3 conditions (Fig. 2J). Therefore, genes that were highly adjustable tended to be associated with CAR-downTSS with promoter.

#### **The CAR-downTSS region was prone to being accessed at mono-nucleosome level, enriched with active histone modifications, and incorporated with histone variant H2a.z**

To further characterize the CAR-downTSS, we calculated fragment size distribution of ATAC-Seq reads within CAR-downTSS and compared it with fragment size distributions within other clusters. A higher frequency of DNA fragments around 150 bps (that is approximately the size of one nucleosome) was detected within CAR-downTSS compared to accessibility regions immediately downstream of TSS (Fig. 3A) or accessibility regions on TSS (Fig. 3B), suggesting CAR-downTSS was prone to being accessed at mono-nucleosome level. To further study the nucleosomes within CAR-downTSS, we performed Cut&Tag sequencing targeting various histone modifications and analyzed their distributions within CAR-downTSS. Cut&Tag sequencing targeting active histone modifications H3K27ac and H3K4me3 showed that both were enriched within CAR-downTSS (Fig. 3C and D) and exhibited fragment size distribution consistent with mono-nucleosome level occupancy (Fig. 3E and F). The enrichment of active histone modification was also verified when analyzed public Chip-Seq data targeting H3K27ac and H3K4me3 (Supplemental Fig. 2B–2 C), while the same dataset showed H3K36me3 was absent within CAR-downTSS (Supplemental Fig. 3D). Meanwhile, Cut&Tag sequencing targeting repressive histone modifications found neither H3K27me3 nor H3K9me3 was enriched in CAR-downTSS (Fig. 3G and

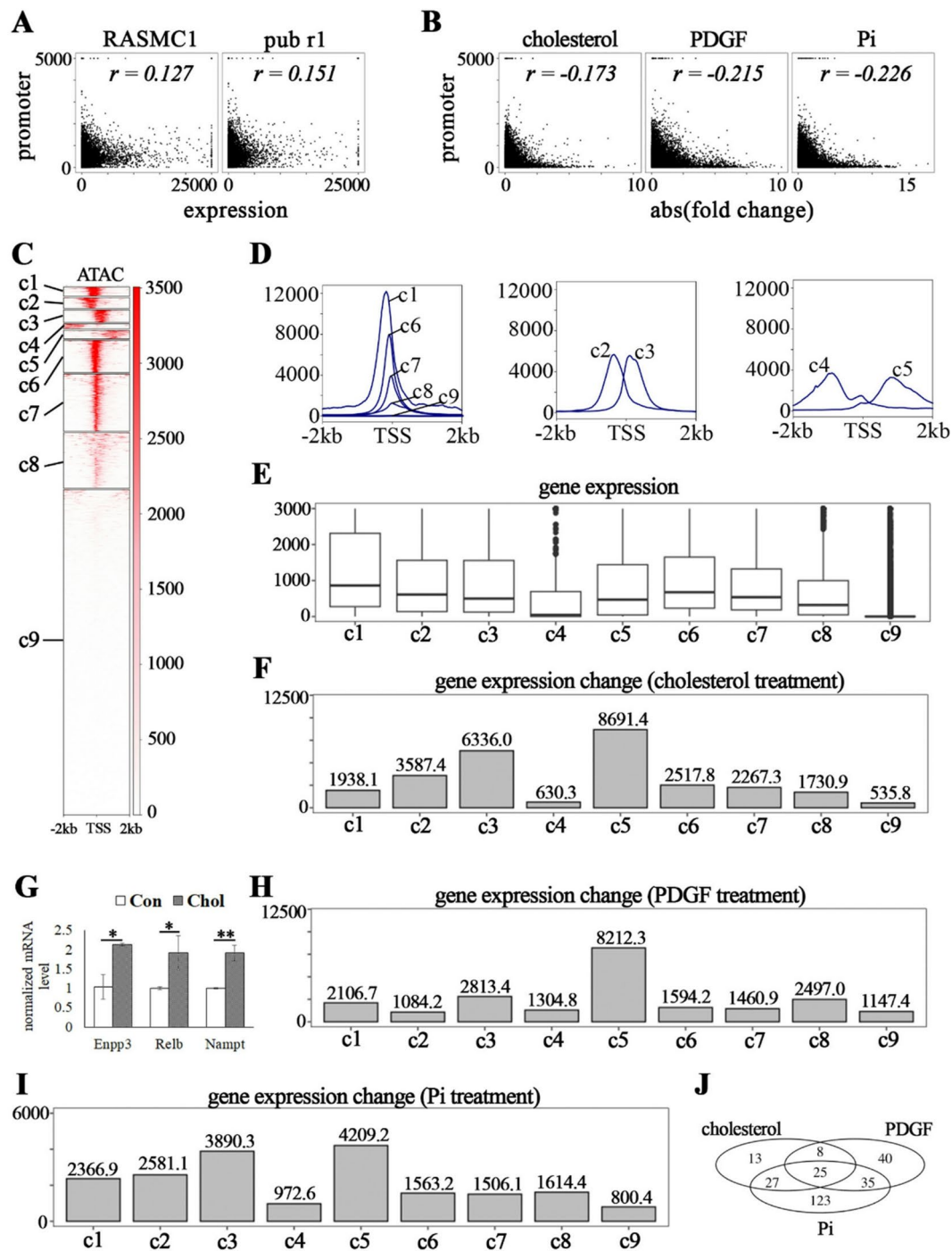


**Fig. 2** Highly adjustable gene tended to be associated with a continuously accessible region downstream of transcription start site (defined as CAR-downTSS). **(A)** Correlation plots showing pairwise Pearson correlation coefficients between promoter accessibility and gene transcription levels. **(B)** Correlation plots showing pairwise Pearson correlation coefficients between promoter accessibility and  $\log_2$ (fold change) values after treatment with cholesterol, PDGF or Pi. **(C)** *k*-means clustering plot of ATAC-Seq signals at genomic regions  $\pm 2000$  bps from transcription start sites. **(D)** Histogram of clusters generated from *k*-means clustering analysis of ATAC-Seq data. **(E)** Box plot showing the expression levels of genes associated with each cluster from *k*-means clustering analysis. **(F)** Cumulative gene expression changes of genes associated each cluster after RASMCs were treated with cholesterol. **(G)** Bar plot showing qRT-PCR results for gene expression changes of *Enpp3*, *Relb* and *Nampt* after RASMCs were treated with cholesterol. **(H-I)** Cumulative gene expression changes after RASMCs were treated with PDGF **(H)** or Pi **(I)**. **(J)** Venn diagram showing overlap of differentially expressed genes associated cluster 5 detected following treatment with cholesterol, PDGF or Pi.

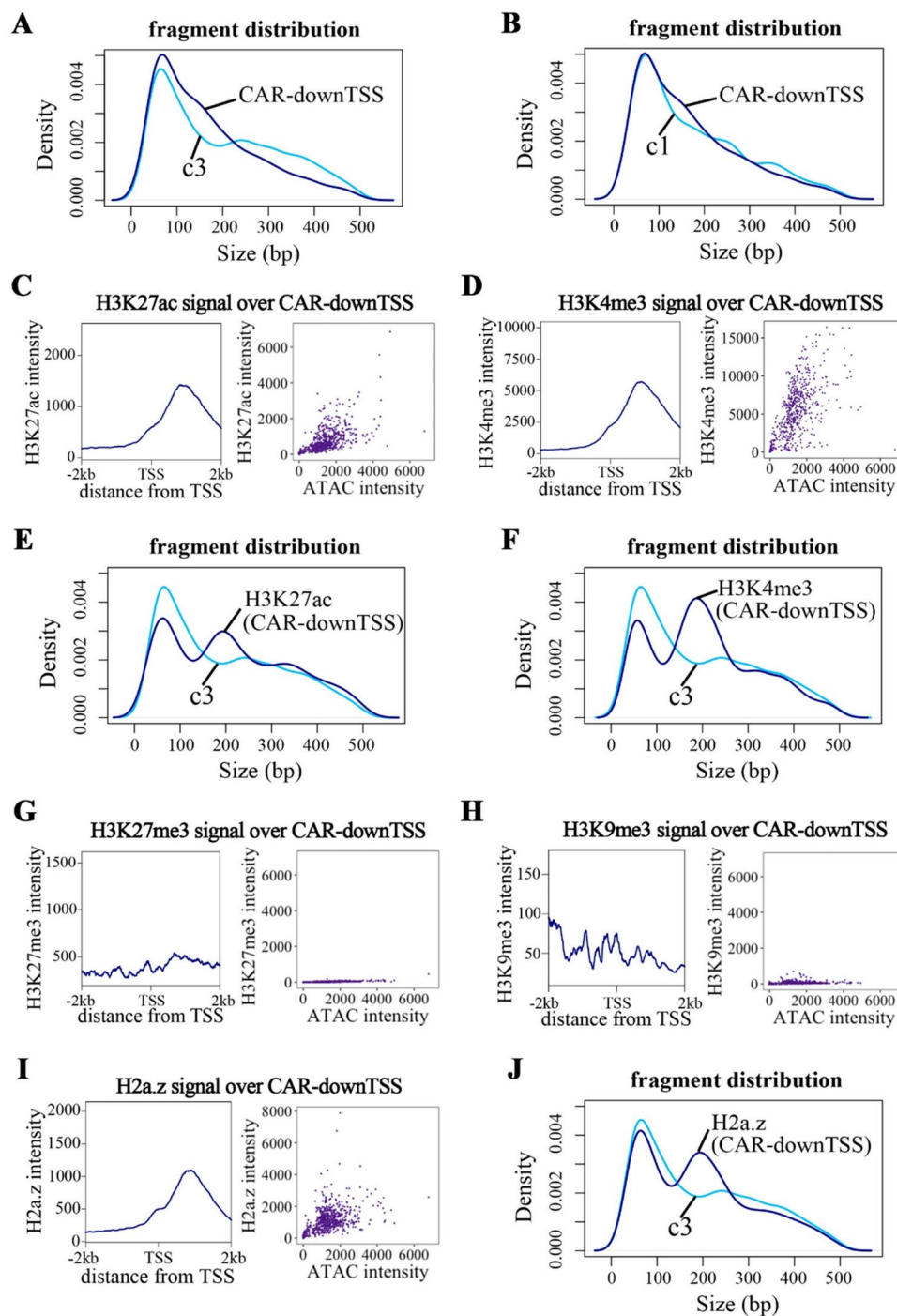


**Fig. 3** The CAR-downTSS region was prone to being accessed at mono-nucleosome level, enriched with active histone modifications, and incorporated with histone variant H2a.z. **(A)** Density plot showing the fragment size distribution of ATAC-Seq reads falling within cluster 5 (CAR-downTSS) and cluster 3. **(B)** Density plot showing the fragment size distribution of ATAC-Seq reads falling within cluster 5 (CAR-downTSS) and cluster 1. **(C-D)** Signal intensity of H3K27ac **(C)** and H3K4me3 **(D)** within CAR-downTSS and its correlation to ATAC-Seq signal. **(E-F)** Density plot showing the fragment size distribution of H3K27ac **(E)** and H3K4me3 **(F)** Cut&Tag sequencing reads falling within CAR-downTSS and cluster 3. **(G-I)** Signal intensity of H3K27me3 **(G)**, H3K9me3 **(H)** and H2a.z **(I)** within CAR-downTSS and its correlation to ATAC-Seq signal. **(J)** Density plot showing the fragment size distribution of H2a.z Cut&Tag sequencing reads falling within CAR-downTSS and cluster 3

H). Therefore, CAR-downTSS was enriched with classic active histone modifications and lack repressive ones. Previous study has shown actively modified nucleosomes located immediately upstream or downstream of TSS relied on histone variant H2a.z to mediate their functions [38]. Here, we also profiled H2a.z distribution via Cut&Tag sequencing and found H2a.z was enriched in CAR-downTSS as well (Fig. 3I) and displayed a fragment size distribution similar to that of active histone modifications (Fig. 3J).

#### **H2a.z was required to maintain the proper chromatin environment within CAR-downTSS and to support the ability of CAR-downTSS-associated genes to increase their expression levels**

To explore the potential role of H2a.z within CAR-downTSS, we used a lentiviral-based shRNA to knock down *H2az1* (the dominant variant of *H2az*) (Fig. 4A). Successful knockdown of H2a.z protein was confirmed via western blot and immunostaining (Fig. 4B). We then further investigated changes in nucleosomes within CAR-downTSS. H3K27ac was significantly reduced, and H3K4me3 was partially reduced within CAR-downTSS following *H2az1* knockdown (Fig. 4C and D). After analyzing the fragment size distribution based on the remaining H3K4me3 Cut&Tag sequencing reads, we also observed a slight shift from 200 bps to 350 bps (resembling the size of di-nucleosome) (Fig. 4E). The fragment size shift caused by *H2az1* knockdown was minor and did not affect the transpassing of RNA polymerase II (Pol II) within CAR-downTSS as Pol II occupancy on CAR-downTSS remained un-changed (Fig. 4F). While, a clear reduction of Pol II within CAR-downTSS was observed when *H2az1*-knockdown cells were further challenged with cholesterol treatment (which by itself had no impact on Pol II) (Fig. 4F).

To further explore the consequences of these changes, we looked into CAR-downTSS-associated genes that had their expression levels increased after cholesterol treatment (Fig. 4G). The ability of these genes to increase their expression in response to cholesterol was significantly reduced after additional *H2az1* knockdown (Fig. 4G). Further qRT-PCR tests were performed to verify the initial gene expression increase in RASMCs transfected with a control (non-targeting) shRNA and the suppression of this increase upon *H2az1* knockdown (Fig. 4H). The reduced ability to increase expression was also demonstrated when *Srcap*, which was known to mediate H2a.z incorporation into nucleosome, was knocked down (Fig. 4I and J). Collectively, these results indicated that H2a.z was required by CAR-downTSS to mediate gene's adjustability. Meanwhile, after assessing the impact of *H2az1* knockdown across other accessibility clusters (Fig. 2C), we also found that although H2a.z

similarly mediated active histone modification (Supplemental Fig. 3), its biological function was influenced by the genomic position into which it was inserted (and also possibly by other factors interacting with these accessible regions). *H2az1* knockdown caused variable changes in chromatin accessibility across different accessibility clusters (Supplemental Fig. 4A-4F), and the insertion of H2a.z into CAR-downTSS specifically promoted a distinctively high capability of gene expression re-adjustment (Supplemental Fig. 4G-4H & Supplemental data 1).

#### **The H2a.z-mediated CAR-downTSS was found to be evolutionarily conserved and could be dynamically re-deployed onto different genes within vascular SMCs**

To verify this H2a.z-supported CAR-downTSS was also conserved in human vascular SMCs, we conducted Cut&Tag sequencing for H2A.Z in HASMC1 and regrouped H2A.Z distribution patterns within promoter regions using k-means clustering. A CAR-downTSS-like distribution of H2A.Z was also observed in HASMC1 and these regions' accessible status was confirmed by ATAC-Seq (Fig. 5A), together suggesting the presence of CAR-downTSS within human vascular SMCs. Similar CAR-downTSS were also detected in HASMC2 and pub h4 (Fig. 5B and C), while they were present in varying quantities: 1 452 promoters in HASMC2 and 896 promoters in puh h4 contained CAR-downTSS compared to 2 097 promoters in HASMC1 (Supplemental data 2). Interestingly, CAR-downTSS was also detected in less plastic cardiomyocytes (Fig. 5D) and played similar gene adjustability-mediating functions (Supplemental Fig. 5A-5B), but adapted in smaller quantities and showed quantitatively stable presence across different samples analyzed (672, 772 and 625 promoters contained CAR-downTSS in sample p1, p2 and p3, respectively) (Fig. 5E & Supplemental data 3). Overlap analysis of genes associated with CAR-downTSS found that most CAR-downTSS-associated genes were shared among the 3 cardiomyocyte samples (Fig. 5E), even though the samples were isolated from patients with a wide age range (2 month old for p1, 3 years old for p2 and 16 years old for p3). Meanwhile, overlap analysis of CAR-downTSS-associated genes detected in different HASMCs showed that only a small portion were shared (Fig. 5F), suggesting CAR-downTSS was dynamically re-deployed onto different genes within plastic vascular SMCs.

#### **Dynamic re-deployment of CAR-downTSS likely occurred in a gene-by-gene manner and was associated with gene's ability to re-adjust its expression level**

To further understand CAR-downTSS in human vascular SMCs, we traced transcriptomic changes in HASMC1 and HASMC2 following cholesterol treatment. *NAMPT*, which was associated with CAR-downTSS and

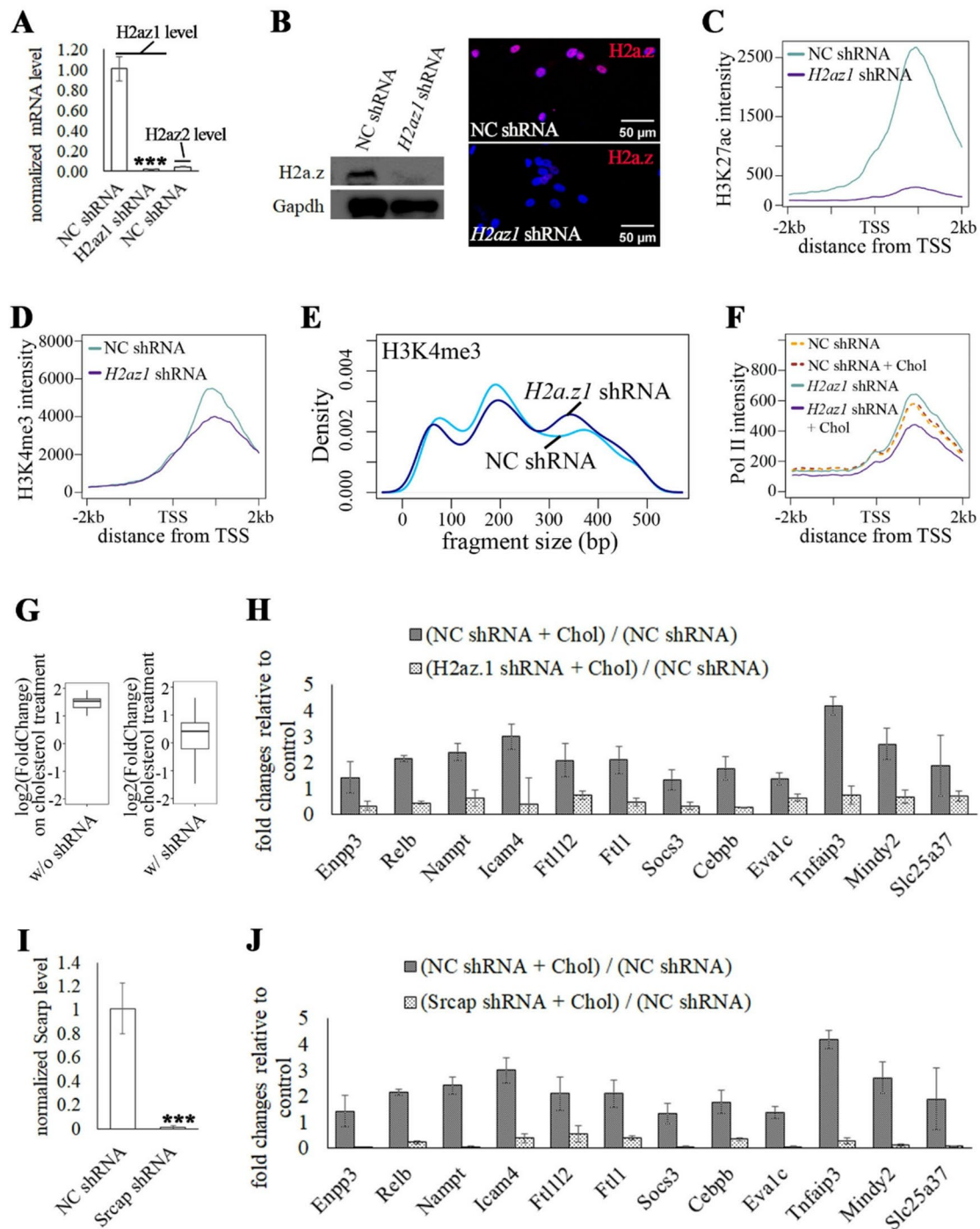


**Fig. 4** H2a.z was required to maintain the proper chromatin environment within CAR-downTSS and to support the ability of CAR-downTSS-associated genes to increase their expression levels. **(A)** Bar plot showing normalized mRNA levels of *H2az1*, *H2az2* after shRNA knockdown of *H2az1* and *H2az2*. **(B)** Western blot and immunostaining results showing *H2a.z* protein was knocked down after shRNA treatment. **(C-D)** Histograms showing signal intensity of H3K27ac **(C)** and H3K4me3 **(D)** within CAR-downTSS before and after *H2a.z* knockdown. **(E)** Density plot showing the fragment size distribution of H3K4me3 Cut&Tag sequencing reads falling within CAR-down before and after *H2a.z* knockdown. **(F)** Histogram showing signal intensity of Pol II within CAR-downTSS before (with or without cholesterol treatment) and after (with or without cholesterol treatment) *H2a.z* knockdown. **(G)** Box plots showing  $\log_2$ (fold change) of genes whose expression were increased after cholesterol treatment (left panel), and  $\log_2$ (fold change) of the same genes under the same condition after additional *H2a.z* knockdown (right panel). **(H)** Bar plot showing fold changes of gene expression after cholesterol treatment with or without *H2a.z* knockdown. **(I)** Bar plot showing normalized *Srcap* mRNA level after *Srcap* shRNA treatment. **(J)** Bar plot showing fold changes of gene expression after cholesterol treatment with or without *Srcap* knockdown

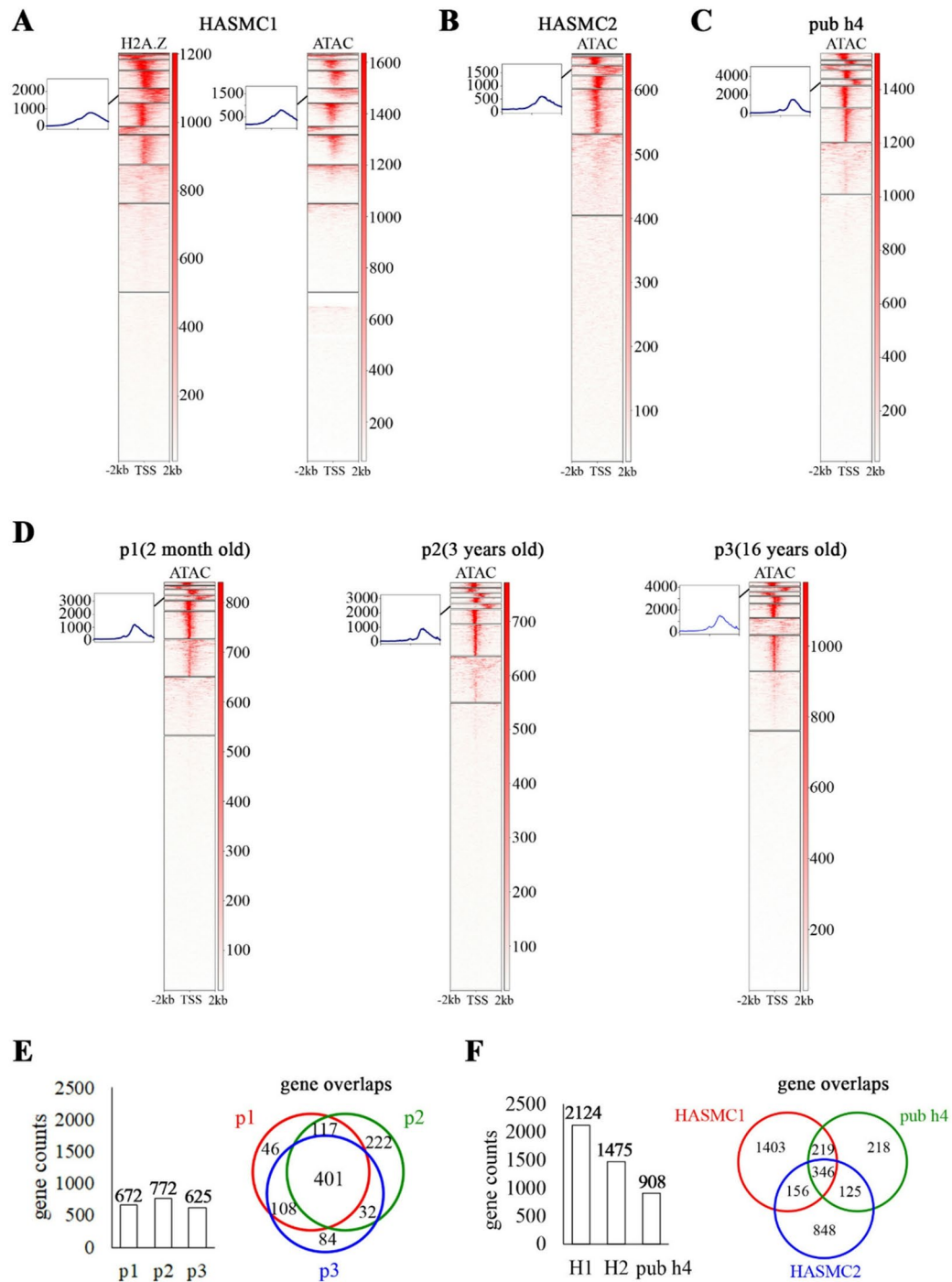


**Fig. 5** The H2a.z-mediated CAR-downTSS was found to be evolutionarily conserved and could be dynamically re-deployed onto different genes within vascular SMCs. **(A)** *k*-means clustering plot of H2A.Z Cut&Tag sequencing signals (left panel) and ATAC-Seq signals (right panel) at genomic regions  $\pm 2000$  bps from transcription start sites in HASMC1. **(B-C)** *k*-means clustering plot of ATAC-Seq signals at genomic regions  $\pm 2000$  bps from transcription start sites in HASMC2 **(B)** and pub h4 **(C)**. **(D)** *k*-means clustering plot of ATAC-Seq signals at genomic regions  $\pm 2000$  bps from transcription start sites in cardiomyocytes. **(E)** Bar plot showing the number of genes associated with CAR-downTSS detected in 3 humans' cardiomyocytes (left panel), and venn diagram showing overlap of these 3 gene groups (right panel). **(F)** Bar plot showing the number of genes associated with CAR-downTSS detected in HASMC1-2 and pub h4 (left panel), and venn diagram showing overlap of these 3 gene groups (right panel)

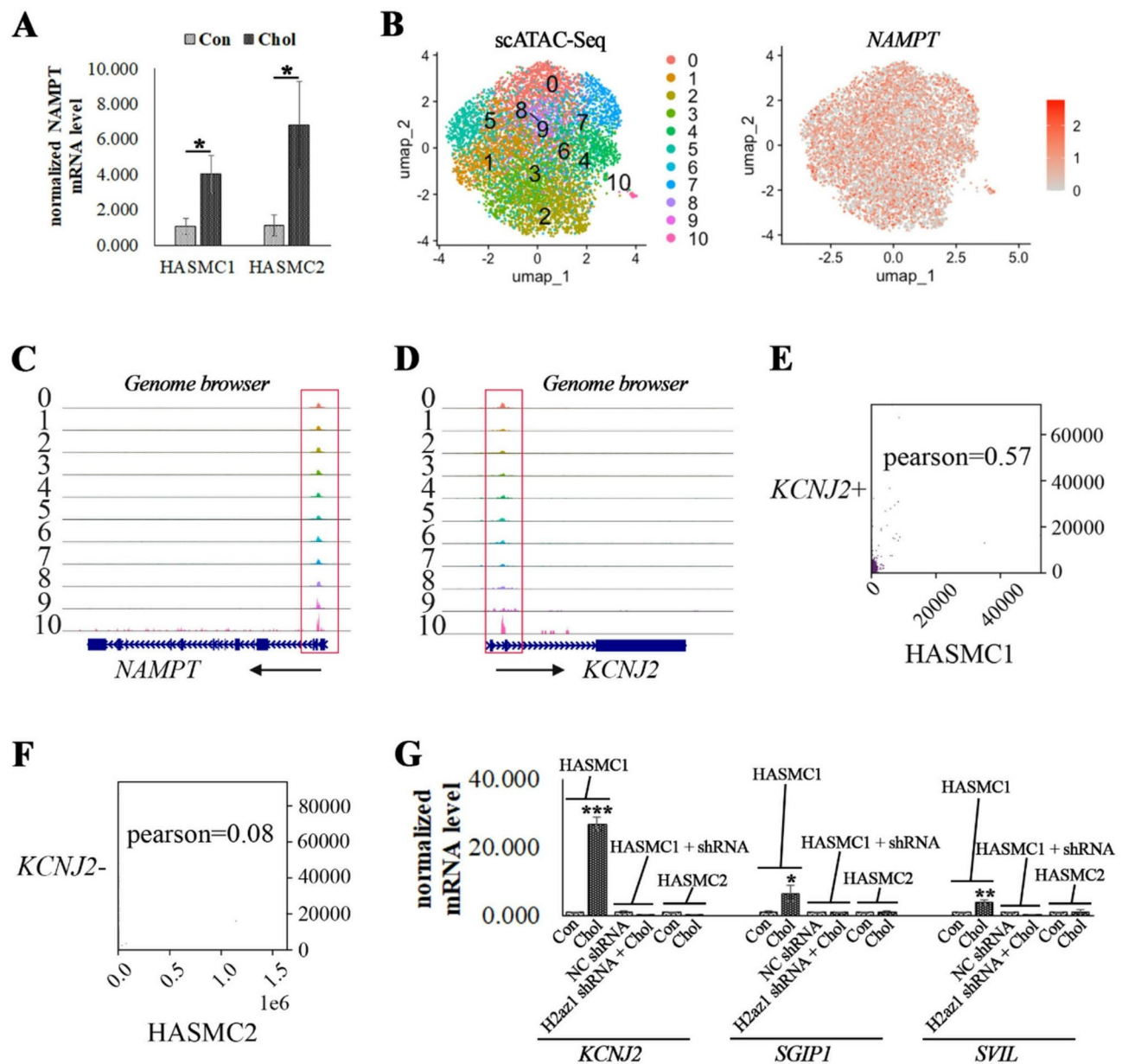


**Fig. 6** Dynamic re-deployment of CAR-downTSS likely occurred in a gene-by-gene manner and was associated with gene’s ability to re-adjust its expression level. **(A)** Bar plot showing normalized *NAMPT* mRNA level in HASMC1-2 after cholesterol treatment. **(B)** UMAP plot showing scATAC-Seq clusters detected in human aortic media (left panel), and accessibility of gene *NAMPT* across these cell clusters (right panel). **(C-D)** Genome coverage plots showing accessible chromatin regions on gene *NAMPT* **(C)** and *KCNJ2* **(D)** across all 10 scATAC-Seq clusters. **(E-F)** Correlation plots showing Pearson correlation coefficients of chromatin accessibility between HASMC1 and *KCNJ2*+ cells separated from scATAC-Seq data **(E)**, and between HASMC2 and *KCNJ2*- cells **(F)**. **(G)** Bar plot showing normalized mRNA level of *KCNJ2*, *SGIP1* and *SVIL* in HASMC1-2 under different conditions

responsive to cholesterol treatment in rat vascular SMCs (Fig. 2G), was also found to be associated with CAR-downTSS in both HASMC lines and similarly responded to cholesterol treatment (Supplemental data 2 &4, Fig. 6A). The conserved adaptation of CAR-downTSS on *NAMPT* was further validated at single-cell level after a human aortic media was processed for scATAC-Seq that revealed similar adaptations of CAR-downTSS across all

HASMCs (Fig. 6B and C), confirming the conservation of CAR-downTSS on this gene.

Meanwhile, gene *KCNJ2*, known to promote vascular SMC proliferation [39], adapted CAR-downTSS only in HASMC1 (Supplemental data 2) and in subset of HASMCs in human aorta (Fig. 6D), suggesting a dynamic adaptation of CAR-downTSS on *KCNJ2*. To further clarify whether CAR-downTSS adaptations were bundled together or occurred in a gene-by-gene

manner, we compared chromatin accessibility between HASMC1 (that adapted CAR-downTSS on *KCNJ2*) and scATAC-Seq sub-clusters with strong adaptation of CAR-downTSS on *KCNJ2*. Poor correlation was observed between these two cell populations (Fig. 6E), and also between HASMC2 (that did not adapt CAR-downTSS on *KCNJ2*) and scATAC-Seq sub-clusters without CAR-downTSS adapted on *KCNJ2* (Fig. 6F), suggesting CAR-downTSS adaptation likely occurred randomly in a gene-by-gene manner. Moreover, the gradually increase of accessibility level on *KCNJ2*'s CAR-downTSS across scATAC-Seq sub clusters (from the lowest on cluster 1, 8 and 9 to the highest on cluster 0 and 10, Fig. 6D) also indicated CAR-downTSS adaptation was a progressive process involving continuous accumulation of active histone modifications and H2A.Z incorporation. Once CAR-downTSS was successfully established (such on *KCNJ2*, *SGIP1* and *SVIL* in HASMC1), genes ability to adjust their expression levels (in case of cholesterol treatment) was significantly increased (Fig. 6G) and these transcriptomic increases relied on histone variant H2A.Z (Fig. 6G & Supplemental Fig. 5C). Therefore, dynamic adaptation of CAR-downTSS played a critical role on supporting gene expression adjustability, which could serve as an important mechanism mediating cellular plasticity.

## Discussion

In the mature human body, certain differentiated cells exhibit a high level of plasticity to fine-tune their cellular functions and maintain homeostasis. However, the mechanisms by which these differentiated cells acquire cellular plasticity remain elusive. Here, through comprehensive transcriptomic and epigenetic studies of highly plastic vascular SMCs, we found that the adjustability of actively transcribed genes was associated with the presence of a continuously accessible region downstream of transcription start site (CAR-downTSS). The CAR-downTSS was located further downstream of Pol II paused region, accessible at mono-nucleosome level and functionally regulated by histone variant H2A.Z. The acquisition of CAR-downTSS was further found to be dynamic in plastic vascular SMCs that could continuously adapt CAR-downTSS onto different genes, while CAR-downTSS was adapted in smaller quantities and remained quantitatively stable in quiescent cardiomyocytes. Thus, dynamic deployment of H2A.Z-mediated CAR-downTSS served as an important mechanism supporting cellular plasticity in vascular SMCs.

H2A.Z is a replication-independent histone variant that is expressed throughout a cell's lifespan, independent of cell mitosis [40, 41]. It is known to maintain a Pol II-paused region immediately downstream of TSS [38, 42, 43] and therefore exhibits enriched signals in this region

[44, 45]. The continued presence of H2A.Z further downstream of TSS was also noticed previously [46] but its function in that context remained unclear. In this study, we found that H2A.Z was incorporated into nucleosomes extending further downstream of TSS, helping to maintain their proper chromatin state including active histone modifications and accessibility at mono-nucleosome level. Depletion of H2A.Z impaired chromatin responses to external stimuli and consequently inhibited the ability of genes to adjust their expression levels. Therefore, the insertion of H2A.Z into nucleosomes continuously downstream of TSS and the resulting formation of a continuously accessible region increased genes' ability to adjust their expression.

The acquisition of CAR-downTSS likely occurred in a gene-by-gene manner in vascular SMCs, as cell populations that had CAR-downTSS formed on the same gene did not share chromatin accessibility profiles in other genomic regions. This gene-by-gene acquisition introduced a degree of randomness in terms of which genes would respond to external stimuli. Such randomness not only aligned with the view that vascular SMC transformation resulted from a combination of gene expression adjustments rather than a programmed transition into predefined cell types [47–49], but also corresponded with the varying SMC transformation processes observed in different systems [50–53]. The most prominent variability would exist among human samples that adapted highly diverse CAR-downTSS profiles across the genome. As shown in this study, genes adapted CAR-downTSS in HASMC1 differed considerably from those in HASMC2 or pub h4 (Supplemental data 2 & 5–7). Future efforts shall be made to collect and compare these epigenetic differences among vascular SMCs from different patients. For example, profiling the chromatin accessibility differences in aortic tissues isolated from patients undergoing aortic dissection repair. This could help to reveal each aorta's potential responsiveness to external stimuli (such as the extent and direction of gene expression changes) based on CAR-downTSS-adapted genes. Such insights could, in turn, inform the design of more personalized monitoring and treatment strategies to better manage vascular health in postoperative care. Meanwhile, we also hope this CAR-downTSS-mediated cellular plasticity could also be utilized to understand the cellular plasticity in other cell systems.

## Conclusions

The plastic vascular SMCs dynamically deployed H2A.Z-positive nucleosomes extending continuously downstream of transcription start sites on different genes to support their transcriptional adjustability, which served as an important mechanism mediating cellular plasticity.

## Supplementary Information

The online version contains supplementary material available at <https://doi.org/10.1186/s12864-025-11679-7>.

Supplementary Material 1  
Supplementary Material 2  
Supplementary Material 3  
Supplementary Material 4  
Supplementary Material 5  
Supplementary Material 6  
Supplementary Material 7  
Supplementary Material 8  
Supplementary Material 9

### Acknowledgements

We thank Dr. Lingjun Jie from Xiamen University and Dr. Guang Li from Southwest Medical University for their valuable discussions on this project. Dr. Lingjun Jie also involved in some experimental processes in this study. We also appreciate the constructive comments from the anonymous reviewers.

### Author contributions

W.S. and J.S. conceived the study. C.Y. conducted the experiments and collected the data. J.H. and Y.W. performed data analysis and actively participated in project discussions. The manuscript was drafted and finalized by W.S.

### Funding

This work is supported by National Natural Science Foundation of China (No. 82200487), Natural Science Foundation of Fujian Province (2024J011427), Xiamen Service for Scholarly Exchange, Health Commission of Xiamen and Xiamen Cardiovascular Hospital of Xiamen University.

### Data availability

All sequencing data generated for this study have been deposited into the Gene Expression Omnibus (GEO) and are accessible under following accession numbers: GSE287684 (secure token: mfyxyiuwlzifnaz) for RNA-Seq of HASMC1, HASMC2 and RASMC1 with or without cholesterol treatment; GSE216071 (secure token: uvuvecwkbrezbkj) for ATAC-Seq of RASMC1; GSE286576 (secure token: qdsnkgmundqtpmb) and GSE287685 (secure token: ezkpcmiclnqdbkf) for Cut&Tag sequencing of H3K27ac, H3K4me3, H3K27me3, H2a.z and pol II in RASMC1; GSE287686 (secure token: qpufyeyozvcbbmb) for RNA-Seq of RASMC1 after H2a.z knockdown; GSE287687 (secure token: kbclqkamzdadbip) for Cut&Tag of H2A.Z and ATAC-Seq of HASMC1; GSE286053 (secure token: elgpyywyvfepdiv) for ATAC-Seq of HASMC2; and GSE286575 (secure token: ejqlcasvnrzryv) for scATAC-Seq of human aortic media. All other public datasets analyzed in this study are described in the Supplemental Methods.

### Declarations

#### Competing interests

The authors declare no competing interests.

Received: 24 January 2025 / Accepted: 6 May 2025

Published online: 19 May 2025

### References

- Broughton KM, Sussman MA. Adult cardiomyocyte cell cycle detour: Off-ramp to quiescent destinations. *Trends Endocrinol Metab.* 2019;30:557–67.
- Garbern JC, Lee RT. Heart regeneration: 20 years of progress and renewed optimism. *Dev Cell.* 2022;57:424–39.
- Wang G, Jacquet L, Karamariti E, Xu Q. Origin and differentiation of vascular smooth muscle cells. *J Physiol.* 2015;593:3013–30.
- Liu Mingjun GD. Smooth Muscle Cell Phenotypic Diversity. *Arteriosclerosis, Thrombosis, and Vascular Biology.* 2019;39:1715–23.
- Bochaton-Piallat M-L, Bäck M. Novel concepts for the role of smooth muscle cells in vascular disease: towards a new smooth muscle cell classification. *Cardiovascular Res.* 2018;114:477–80.
- Durham AL, Speer MY, Scatena M, Giachelli CM, Shanahan CM. Role of smooth muscle cells in vascular calcification: implications in atherosclerosis and arterial stiffness. *Cardiovasc Res.* 2018;114:590–600.
- Miano JM, Fisher EA, Majesky MW. Fate and state of vascular smooth muscle cells in atherosclerosis. *Circulation.* 2021;143:2110–6.
- Petsophonsakul P, Furmanik M, Forsythe R, Dweck M, Schurink GW, Natour E, Arteriosclerosis, et al. *Thromb Vascular Biology.* 2019;39:1351–68.
- Gomez D, Owens GK. Smooth muscle cell phenotypic switching in atherosclerosis. *Cardiovascular Res.* 2012;95:156–64.
- Chen P-Y, Qin L, Li G, Malagon-Lopez J, Wang Z, Bergaya S, et al. Smooth muscle cell reprogramming in aortic aneurysms. *Cell Stem Cell.* 2020;26:542–e55711.
- Bennett MR, Sinha S, Owens GK. Vascular smooth muscle cells in atherosclerosis. *Circ Res.* 2016;118:692–702.
- Haberle V, Lenhard B. Promoter architectures and developmental gene regulation. *Semin Cell Dev Biol.* 2016;57:11–23.
- Pollex T, Rabinowitz A, Gambetta MC, Marco-Ferreres R, Viales RR, Jankowski A, et al. Enhancer-promoter interactions become more instructive in the transition from cell-fate specification to tissue differentiation. *Nat Genet.* 2024;56:686–96.
- Chen H, Pugh BF. What do transcription factors interact with?? *J Mol Biol.* 2021;433:166883.
- Saltzman AG, Weinmann R. Promoter specificity and modulation of RNA polymerase II transcription. *FASEB J.* 1989;3:1723–33.
- Kornberg RD, Lorch Y. Primary role of the nucleosome. *Mol Cell.* 2020;79:371–5.
- Karlič R, Chung H-R, Lasserre J, Vlahovick K, Vingron M. Histone modification levels are predictive for gene expression. *Proc Natl Acad Sci U S A.* 2010;107:2926–31.
- Guillemette B, Bataille AR, Gévry N, Adam M, Blanchette M, Robert F, et al. Variant histone H2A.Z is globally localized to the promoters of inactive yeast genes and regulates nucleosome positioning. *PLoS Biol.* 2005;3:e384.
- Liu X, Zhang J, Zhou J, Bu G, Zhu W, He H, et al. Hierarchical accumulation of histone variant H2A.Z regulates transcriptional states and histone modifications in early mammalian embryos. *Adv Sci (Weinh).* 2022;9:e2200057.
- Satpathy AT, Granja JM, Yost KE, Qi Y, Meschi F, McDermott GP, et al. Massively parallel single-cell chromatin landscapes of human immune cell development and intratumoral T cell exhaustion. *Nat Biotechnol.* 2019;37:925–36.
- Hao Y, Hao S, Andersen-Nissen E, Mauck WM, Zheng S, Butler A, et al. Integrated analysis of multimodal single-cell data. *Cell.* 2021;184:3573–e358729.
- Stuart T, Srivastava A, Madad S, Lareau CA, Satija R. Single-cell chromatin state analysis with Signac. *Nat Methods.* 2021;18:1333–41.
- Chen S, Zhou Y, Chen Y, Gu J. Fastp: an ultra-fast all-in-one FASTQ preprocessor. *Bioinformatics.* 2018;34:i884–90.
- Langmead B, Salzberg SL. Fast gapped-read alignment with bowtie 2. *Nat Methods.* 2012;9:357–9.
- Li H, Handsaker B, Wysoker A, Fennell T, Ruan J, Homer N, et al. The sequence alignment/map format and samtools. *Bioinformatics.* 2009;25:2078–9.
- Ramirez F, Dündar F, Diehl S, Grüning BA, Manke T. DeepTools: a flexible platform for exploring deep-sequencing data. *Nucleic Acids Res.* 2014;42:187–91. Web Server issue:W.
- Dobin A, Davis CA, Schlesinger F, Drenkow J, Zaleski C, Jha S, et al. STAR: ultrafast universal RNA-seq aligner. *Bioinformatics.* 2013;29:15–21.
- Anders S, Pyl PT, Huber W. HTSeq—a Python framework to work with high-throughput sequencing data. *Bioinformatics.* 2015;31:166–9.
- Love MI, Huber W, Anders S. Moderated Estimation of fold change and dispersion for RNA-seq data with DESeq2. *Genome Biol.* 2014;15:550.
- Rong JX, Shapiro M, Trogan E, Fisher EA. Transdifferentiation of mouse aortic smooth muscle cells to a macrophage-like state after cholesterol loading. *Proceedings of the National Academy of Sciences.* 2003;100:13531–6.
- Wong KHY, Levy-Sakin M, Kwok P-Y. De Novo human genome assemblies reveal spectrum of alternative haplotypes in diverse populations. *Nat Commun.* 2018;9:3040.
- Kulski JK, Suzuki S, Shiina T. Human leukocyte antigen super-locus: nexus of genomic supergenes, SNPs, Indels, transcripts, and haplotypes. *Hum Genome Var.* 2022;9:1–15.

33. PDGF-BB-mediated. Activation of CREB in vascular smooth muscle cells alters cell cycling via Rb, FoxO1 and p27kip1. *Exp Cell Res.* 2021;404:112612.
34. Li J, Li C, Huang Z, Huang C, Liu J, Wu T, et al. Empagliflozin alleviates atherosclerotic calcification by inhibiting osteogenic differentiation of vascular smooth muscle cells. *Front Pharmacol.* 2023;14:1295463.
35. Zhou M, Qi L, Gu Y. GRIA2/ENPP3 regulates the proliferation and migration of vascular smooth muscle cells in the restenosis process Post-PTA in lower extremity arteries. *Front Physiol.* 2021;12:712400.
36. RelB. Represses miR-193a-5p expression to promote the phenotypic transformation of vascular smooth muscle cells in aortic aneurysm. *Biochim Et Biophys Acta (BBA) - Gene Regul Mech.* 2023;1866:194926.
37. Li D, Chen Y, Wang Y, Liu J, Chai L, Zhang Q, et al. NAMPT mediates PDGF-induced pulmonary arterial smooth muscle cell proliferation by TLR4/NF- $\kappa$ B/PLK4 signaling pathway. *Eur J Pharmacol.* 2023;961:176151.
38. Liu X, Zhang J, Zhou J, Bu G, Zhu W, He H, et al. Hierarchical accumulation of histone variant H2A.Z regulates transcriptional States and histone modifications in early mammalian embryos. *Adv Sci.* 2022;9:2200057.
39. Cao N, Aikeremu N, Shi W-Y, Tang X-C, Gao R-J, Kong L-J-Y, et al. Inhibition of KIR2.1 decreases pulmonary artery smooth muscle cell proliferation and migration. *Int J Mol Med.* 2022;50:119.
40. Giaimo BD, Ferrante F, Herchenröther A, Hake SB, Borggreffe T. The histone variant H2A.Z in gene regulation. *Epigenetics Chromatin.* 2019;12:37.
41. H2A.Z. Histone variants facilitate HDACi-dependent removal of H3.3K27M mutant protein in pediatric high-grade glioma cells. *Cell Rep.* 2024;43:113707.
42. The H2A. Z-nucleosome code in mammals: emerging functions. *Trends Genet.* 2022;38:273–89.
43. Recoules L, Heurteau A, Raynal F, Karasu N, Moutahir F, Bejjani F et al. The histone variant macroH2A1.1 regulates RNA polymerase II-paused genes within defined chromatin interaction landscapes. *J Cell Sci.* 2022;135.
44. Neves LT, Douglass S, Spreafico R, Venkataramanan S, Kress TL, Johnson TL. The histone variant H2A.Z promotes efficient cotranscriptional splicing in *S. cerevisiae*. *Genes Dev.* 2017;31:702–17.
45. Bargaje R, Alam MP, Patowary A, Sarkar M, Ali T, Gupta S, et al. Proximity of H2A.Z containing nucleosome to the transcription start site influences gene expression levels in the mammalian liver and brain. *Nucleic Acids Res.* 2012;40:8965–78.
46. Cole L, Kurscheid S, Nekrasov M, Domaschenz R, Vera DL, Dennis JH, et al. Multiple roles of H2A.Z in regulating promoter chromatin architecture in human cells. *Nat Commun.* 2021;12:2524.
47. Sorokin V, Vickneson K, Kofidis T, Woo CC, Lin XY, Foo R, et al. Role of vascular smooth muscle cell plasticity and interactions in vessel wall inflammation. *Front Immunol.* 2020;11:599415.
48. Regulation of vascular. Smooth muscle cell differentiation. *J Vasc Surg.* 2007;45:A25–32.
49. Perry RN, Albarracin D, Aherrahrou R, Civelek M. Network Preservation Analysis Reveals Dysregulated Metabolic Pathways in Human Vascular Smooth Muscle Cell Phenotypic Switching. *Circulation: Genomic and Precision Medicine.* 2023;16:372–81.
50. Zhang Z, Huang J, Wang Y, Shen W. Transcriptome analysis revealed a two-step transformation of vascular smooth muscle cells to macrophage-like cells. *Atherosclerosis.* 2022;346:26–35.
51. Swirski FK, Nahrendorf M. Do vascular smooth muscle cells differentiate to macrophages in atherosclerotic lesions? *Circ Res.* 2014;115:605–6.
52. Alencar GF, Owsiany KM, Karnewar S, Sukhavasi K, Mocci G, Nguyen AT, et al. Stem cell pluripotency genes Klf4 and Oct4 regulate complex SMC phenotypic changes critical in Late-Stage atherosclerotic lesion pathogenesis. *Circulation.* 2020;142:2045–59.
53. Li Y, Zhu H, Zhang Q, Han X, Zhang Z, Shen L, et al. Smooth muscle-derived macrophage-like cells contribute to multiple cell lineages in the atherosclerotic plaque. *Cell Discov.* 2021;7:1–4.

#### Publisher's note

Springer Nature remains neutral with regard to jurisdictional claims in published maps and institutional affiliations.